Structure of copper tellurite and borotellurite glasses by neutron diffraction, Raman, ^{11}B MAS-NMR and FTIR spectroscopy

Amandeep Kaur,[a] *Atul Khanna,*[a1] *P. S. R. Krishna,*[b] *A. B. Shinde,*[b] *Marina González-Barriuso,*[c] *Fernando González*[c] *& Banghao Chen*[d]

[a] *Department of Physics, Guru Nanak Dev University, Amritsar-143005, Punjab, India*
[b] *Solid State Physics Division, Bhabha Atomic Research Centre, Mumbai-400085,Maharashtra, India*
[c] *Department of Chemistry and Process & Recourse Engineering, University of Cantabria, Spain*
[d] *Chemistry & Biochemistry Department, Florida State University, Tallahassee, FL 32306, USA*

Manuscript received 9 June 2018
Revision received 9 February 2019
Manuscript accepted 11 March 2019

The structure of copper tellurite and borotellurite glasses is studied by x-ray and neutron diffraction, reverse Monte Carlo (RMC) simulations, FTIR, Raman and ^{11}B MAS-NMR spectroscopy. Copper tellurite sample with 15 mol% CuO forms precipitates of tetragonal TeO_2 within the glass matrix on melt quenching. The glass forming ability of the $xCuO–(100–x)TeO_2$ system enhances with increase in CuO concentration from 15 to 20 mol% and also with the addition of B_2O_3. RMC simulations on the neutron diffraction data found that the Cu–O and Te–O bond lengths are approximately at equal distances in the range: 1·96 to 1·98±0·02 Å, while the nearest O–O distance is at 2·71±0·02 Å. Neutron and Raman results on the Te–O speciation are in agreement and confirmed that the Te–O coordination decreases with an increase in CuO and B_2O_3 molar concentrations in the tellurite and borotellurite glasses, respectively. RMC studies found that Cu^{2+} has tetrahedral coordination with oxygen, as predicted by Jahn–Teller distortion and that Cu–O and Te–O structural units have very similar size and geometry. The copper tellurite glass-ceramic sample with 15 mol% CuO was heat treated and it formed crystalline precipitates of TeO_2 and $CuTe_2O_5$ upon devitrification; the average Te–O coordination was significantly smaller in the glass as compared to that in the crystalline sample.

1. Introduction

Tellurite glasses have several attractive properties such as high refractive indices, low melting points, low phonon energies, high dielectric constants and high transmittance from visible to the near-infrared range of the electromagnetic spectrum; and have applications in nonlinear optical devices for second and third harmonic generation and in optical waveguides for light communication.[1–4] Tellurite glasses and glass ceramics that contain transition metal oxides such as CuO and V_2O_5 are semiconducting and show significant electronic conduction and have potential electrochemical applications as cathode materials in secondary batteries.[5–7]

TeO_4 and TeO_3 are the basic structural units of the tellurite glass network and both these structural units contain a lone pair of electrons at the equatorial sites.[8,9] The addition of transition metal oxides in tellurite glasses modifies the structure by forming new ionic bonds and creates nonbridging oxygens that affect the electrical conductivity, thermal stability and optical properties of glasses.[10–13] The addition of metal ions elongates one oxygen–tellurium linkage in TeO_4 and forms TeO_{3+1} and TeO_3 structural units.[14–16] It is important to determine the structural properties of tellurite glasses; in particular the Te^{4+} and the modifier ion co-ordination environment, bond lengths, nearest neighbour distances and the bond angle distributions to model the mechanical, optical, thermal, electrical and magnetic properties of glasses. Several techniques such as x-ray and neutron diffraction,[9,14,17] x-ray photoelectron spectroscopy(XPS),[18] *ab initio* calculations,[19] and Raman spectroscopy[1,9] have been used for the structural studies of tellurite glasses and crystals. Te–O co-ordination is an important structural parameter that also influences the glass forming ability (GFA) of the tellurite materials.

Copper can exist as Cu^+, Cu^{2+} and Cu^0 in oxide glasses.[20–22] At low concentration of CuO doping in $Li_2O–MoO_3–B_2O_3$ glasses, it is reported that mostly Cu^{2+} are present and that on increasing CuO concentration beyond 0·6 mol%, the Cu^{2+} reduce to Cu^+.[21] The increase in CuO concentration in the glass series: $(35–x)Pb_3O_4–xCuO–65Li_2B_4O_7$ is found to exhibit the structural transformation: $BO_4 \rightarrow BO_3$. Glasses that contain CuO have interesting electrical and magnetic properties.[23] xCuO–(100–x)TeO_2 glasses show

[1] Corresponding author. Email atul.phy@gndu.ac.in
DOI: 10.13036/17533562.61.1.007

antiferromagnetic and ferromagnetic interactions among the Cu^{2+} ions.[24,25] Like gold nanoparticles, Cu^{2+} and Cu^{+} can be used to produce ruby-glass, Cu^{+} in glasses can be oxidised to Cu^{2+} by the photochemical reaction and this property can be used to synthesise photochromatic materials.[26] Therefore CuO doping in oxide glasses has important optical applications. The addition of Cu^{2+} in lead and zinc borate glasses is reported to enhance the packing density, glass transition temperature and mechanical hardness and the elastic moduli.[27] Similar effects of doping with Cu^{2+} is reported on the optical and thermal properties of $(50-x/2)Na_2O$–xCuO–$(50-x/2)$ P_2O_5 glasses.[28]

Cu^{2+} ions are expected to have octahedral coordination with oxygens in crystalline compounds, complexes and glasses, however, due to Jahn–Teller (JT) distortion, the Cu–O coordination decreases from 6 to 4.[28–30] For instance, in $[Cu(H_2O)_6]^{2+}$ the two Cu–O linkages elongate from a length of 2·00 to 2·45 Å and the Cu–O site transforms from the elongated octahedral to tetrahedral. It is well known that the metal ions with coordination number of three or four can act as a network formers whereas the cations with higher coordination numbers of 6 or more act as network modifiers.[31] It is therefore very interesting to study the speciation (coordination environment) of Cu^{2+} in oxide glasses. Electron paramagnetic resonance (EPR) studies on sodium phosphate glasses containing Cu^{2+} showed that these ions have tetrahedrally elongated octahedral sites in certain phosphate glasses.[32] Neutron diffraction is however the direct and the most suitable method to study the coordination environment of the metal ions in oxide glasses.

TeO_2 is a conditional glass former that forms glassy phase only at high melt quenching rates of ~10^5 K/s,[9,33] however when it is mixed with alkali, alkaline earth, transition and heavy metal oxides it forms glasses rather easily at moderate quenching rates of ~10^2–10^3 K/s.[3] The other good glass formers such as SiO_2 or B_2O_3 form glasses with CuO only in the presence of a third component such as alkali and heavy metal oxides.[27,32,34] TeO_2, on the contrary forms binary glasses in the wide composition range with a variety of metal oxides including CuO,[3,24,35] therefore in the present work, TeO_2 is used as a network former to prepare glasses from the xCuO–$(100-x)TeO_2$ system with the primary aim to study the changes in Cu–O and Te–O speciation with glass composition. Glasses from this system are reported to be semiconducting with an electrical conductivity that is three to four orders of magnitude higher than that of copper phosphate glasses with equal CuO concentration.[36] The incorporation of a second glass former such as B_2O_3 into the tellurite network leads to a complex glass structure that consists of borate, tellurite and mixed structural units. B_2O_3 is an excellent glass former which increases the GFA, thermal stability and the ultraviolet–visible transmittance of the tellurite glasses.[37,38] On increasing B_2O_3 concentration in tellurite glasses, it is reported that the tetrahedral borons transform into the triangular boron units.[39]

In the present study, copper tellurite glass and glass-ceramic samples were prepared and their short range and medium range order properties were studied by neutron diffraction and Raman spectroscopy. Reverse Monte-Carlo (RMC) simulations of the neutron scattering data of two copper tellurite glasses were performed and the partial pair correlation functions, Te–O and Cu–O coordinations and the bond angle distributions of the cation–oxygen linkages were determined. Further, the effects of the addition of the second network former (B_2O_3) on B–O and Te–O speciation, and on the glass thermal properties were studied by ^{11}B magic angle spinning nuclear magnetic resonance (MAS-NMR), Fourier transform infrared (FTIR), Raman spectroscopy and differential scanning calorimetry (DSC) techniques, respectively. Finally, the short range structure of one copper tellurite glass sample and its devitrified (crystallised) sample are compared.

2. Experimental

2.1. Glass preparation and devitrification

Copper tellurite and copper borotellurite glasses from the two systems (i) xCuO–$(100-x)$ TeO_2 (where x=15 and 20 mol%) and (ii) 20CuO–$y$$B_2O_3$–$(100-y)$ TeO_2 (y=10, 20 and 30 mol%) were prepared by melt quenching using CuO (Central Drug House, India, 98%), H_3BO_3 (Aldrich, India, 99·9%) and TeO_2 (Aldrich, India, 99%) as starting materials. Appropriate amounts of these materials were weighed, mixed together and transferred in a platinum crucible and melted at 900°C for 30 min in a muffle furnace. Samples were prepared by splat quenching in which the melt was pressed between two steel plates and dark green colored samples were obtained.

Copper tellurite glass with 15 mol% CuO (15CuTe) was annealed at 380°C (higher than its glass transition temperature (T_g)) for 4 h in air to devitrify it. The composition and density of the samples are given in Table 1.

2.2. X-ray diffraction (XRD)

XRD studies were performed on powdered glass samples on Bruker D8 Focus x-ray diffractometer

Table 1. Composition, density and atomic number density of copper tellurite and borotellurite glasses

Sample code	*Composition (mol%)*			*Density, ρ (g/cm³) ±0·05*	*Atomic number density ρ_o (Å^{-3})*
	CuO	*B_2O_3*	*TeO_2*		
15CuTe	15	-	85	5·61	0·0653
20CuTe	20	-	80	5·66	0·0665
20Cu10BTe	20	10	70	5·11	0·0681
20Cu20BTe	20	20	60	4·71	0·0722
20Cu30BTe	20	30	50	4·51	0·0792

with Cu K_α radiation (λ=1·54056 Å) in the 2θ range of 10–65°. The x-ray tube was operated at 40 kV and 30 mA and the scattered x-ray intensity was measured with the scintillation detector.

2.3. Density measurement

The densities of glass samples was measured by Archimedes method using dibutylphatalate (DBP) as the immersion fluid and are given in Table 1. The maximum error in the densities is ±0·05 g/cm^3.

2.4. Differential scanning calorimetry (DSC)

DSC studies were carried out using SETARAM SETSYS 16 TG-DSC system in the temperature range of 200–800°C at a heating rate of 10°C/min. Measurements were performed on the powdered samples kept in platinum pans. Samples amounts of 20–50 mg were used for DSC analysis. The maximum uncertainty in the measurement of glass transition (mid-point), crystallisation (peak point) and melting temperatures (peak point) is ±1°C (Table 2).

2.5. Neutron diffraction

Neutron diffraction studies were carried out on two copper tellurite glass samples using monochromatic neutrons of de-Broglie wavelength, λ=0·783 Å at the Dhruva reactor of Bhabha Atomic Research Centre, Trombay, Mumbai, India. These studies were done on the pulverised samples kept in vanadium cans in the momentum transfer, Q-range: 1·0 to 14·3 Å^{-1}. RMC simulations were performed on the neutron scattering data using RMC^{++} software,[40,41] and the partial pair correlation functions, bond lengths/nearest neighbour distances, Te–O and Cu–O coordinations and bond angle distributions were found from the RMC analysis.

2.6. RMC simulations

The neutron scattering data were corrected for background, multiple scattering and absorption and normalized with vanadium.[42–46] The experimental neutron structure factor $S(Q)$ data was obtained and simulated by the RMC method using RMC^{++} Version 1.5.1 software package to generate the partial pair correlation functions, coordination numbers and the O–Te–O, O–Cu–O and O–O–O bond-angle distributions.[40,47]

The RMC technique minimises the squared difference between the experimental $S(Q)$ and the simulated one from a three-dimensional atomic configuration and partial correlation functions $g_{ij}(r)$ and the neutron scattering weight factors for different correlations were calculated by the following formulas:[48–53]

$$S(Q) = \sum_{i,j}^{k} w_{ij} S_{ij}(Q) \quad (1)$$

$$S_{ij}(Q) = 1 + \frac{4\pi\rho_o}{Q} \int_0^{r_{max}} r\left[g_{ij}(r) - 1\right] \sin Qr \, dr \quad (2)$$

$$w_{ij} = \frac{c_i b_i c_j b_j \left(2 - \delta_{ij}\right)}{\left[\sum_i^k c_i b_i\right]^2} \quad (3)$$

where δ_{ij} is the Kroneker delta function; c_i, c_j are the molar fractions of the i-th and j-th atoms in the sample, respectively; b_i, b_j are the corresponding neutron coherent scattering lengths; and k is the total number of elements in the sample and calculated data is given in Table 3. The RMC simulation calculates the one-dimensional partial atomic pair correlation functions $g_{ij}(r)$, and these are Fourier transformed to calculate the partial structure factors, $S_{ij}(Q)$. The disordered atomic configuration was first built up to run the RMC program with a simulation box that contained 10 000 atoms. The atomic number density values were 0·0653 and 0·0665 Å^{-3} and the RMC model box lengths were 26·753 Å and 26·588 Å for the two samples: 15CuTe and 20CuTe, respectively (Table 1).

During the RMC simulations, the minimum interatomic distances constraints (cut-off distances) were used to fit the model with experimental $S(Q)$. No other constraints (such as co-ordination constraints) were applied during RMC simulations. Repeated RMC runs were performed by modifying the values of cut-off distances in such a way that it produced reliable data for each pair correlation function, $g_{ij}(r)$ and coordination number, CN_{ij}. The final cut-off distances used in the RMC program for Cu–Cu, Cu–Te, Cu–O, Te–Te, Te–O and O–O correlations were 2·30, 2·60, 1·60, 2·20, 1·60 and 2·35 Å, respectively, for the two copper tellurite samples and, the average coordination numbers of Te, Cu and O with O were obtained from RMC analysis. The r_{max} and r_{min} values of the partial pair correlation functions that were used for

Table 2. Thermal properties of copper tellurite and borotellurite glasses

Sample code	T_g (°C)	T_c (°C) T_{c1}	T_{c2}	T_m (°C) T_{m1}	T_{m2}	$\Delta T = T_c - T_g$ (°C)	E_B (kJ/mol)
15CuTe	306	362	-	-	-	56	384
20CuTe	301	381	457	615	-	80	381
20Cu10BTe	325	464	-	574	613	138	423
20Cu20BTe	333	504	-	586	-	171	465
20Cu30BTe	366	520	-	556	-	154	506

Table 3. Neutron scattering weight factors (%) in CuO–TeO_2 glasses

	Atom pair	*15CuTe*	*20CuTe*
Neutron	Cu–Cu	0·47	0·99
weight factors	Cu–Te	4·04	5·98
w_{ij} (%)	Cu–O	8·79	11·97
	Te–Te	8·58	8·99
	Te–O	37·39	36·01
	O–O	40·71	36·03

calculating the coordination number distributions for Te–O, Cu–O and O–O atom pairs are given in Table 4.

2.7. Raman spectroscopy

Raman scattering studies were performed on the samples with Renishaw In-Via Reflex micro-Raman spectrometer using 514·5 nm argon ion laser (50 mW) as the excitation source, a diffraction grating having 2400 lines/mm, an edge filter for Stokes spectra and a Peltier cooled CCD detector. Measurements were carried out in an unpolarised mode at room temperature in the backscattering geometry, in the wave-number range: 30 to 1000 cm^{-1} at a spectral resolution of better than 1 cm^{-1}.

2.8. ^{11}B MAS-NMR

^{11}B MAS–NMR studies were performed on copper borotellurite glasses on Bruker AVIII HD NMR spectrometer operating at a magnetic field of 11·74 T with a 4 mm Bruker MAS probe at Larmor frequency of 160·5299 MHz for ^{11}B nuclei. Sample spinning rate was 14 kHz. Short RF pulses (<15°) with recycle delay of 20 s were used. Spectra were collected after 4096 scans and referenced to solid $NaBH_4$ at −42·16 ppm.

2.9. FTIR

The FTIR spectra of copper tellurite and borotellurite glasses were recorded on Bruker Vertex FTIR spectrophotometer using KBr disk technique in the wavenumber range: 400 to 2000 cm^{-1} at room temperature. The mixture of powdered glass sample and spectroscopic grade KBr (1:100 by weight) was subjected to a pressure of 10 ton/cm^2 to prepare thin pellets. The FTIR absorption spectra were measured immediately after preparing the pellets.

3. Results and discussion

3.1 X-ray diffraction

The XRD pattern of the sample that contained 15 mol% CuO shows a broad hump and several sharp peaks centered at 26·4, 28·9, 30·0, 37·4, 48·7, 54·0, 55·4, 61·0, 62·4 and 63·0° which match with the tetragonal α-TeO_2 phase.[54] This sample is a mostly glassy phase with a small concentration of crystalline precipitates of tetragonal TeO_2. After annealing this sample at 380°C in air for 4 h (Sample Code: 15CuTe-CR), crystallinity increases significantly and several new sharp peaks were detected in the XRD pattern; which match with the tetragonal TeO_2 and the monoclinic $CuTe_2O_5$ phases,[55] the later phase shows peaks at 22·8, 27·5, 29·2, 36·7, 42·8, 46·9, 51·0 and 57·7° (Figure 1). Crystalline $CuTe_2O_5$ and TeO_2 phases are produced by the following crystallisation (devitrification) reaction with heat treatment:

$$15CuO–75TeO_2 \rightarrow 15CuTe_2O_5+45TeO_2 \quad (4)$$

It may be noted that the devitrified sample (15CuTe-CR) is also not fully crystalline, but contains a significant amount of the remnant glassy phase as evidenced by the broad hump in its XRD pattern (Figure 1).

Copper tellurite sample with 20 mol% CuO (20CuTe) and all the copper borotellurite samples show only broad humps in the 2θ range of 20° to 30° without any sharp peaks (Figure 2). The absence of sharp peaks confirms the amorphous nature of these samples. Clearly, the glass-forming ability (GFA) of the xCuO–(100−x)TeO_2 system is enhanced with an increase in CuO concentration from 15 to 20 mol%. The enhancement of GFA is also confirmed by the steady increase in thermal stability, $\Delta T=(T_c-T_g)$ with increase in both CuO and B_2O_3 mol% (Table 2), as found by DSC analysis (discussed below).

Table 4. The r_{min} and r_{max} values used to calculate the Cu–O, Te–O and O–O coordination by RMC simulations

Sample code	Cu–O		Te–O		O–O	
	r_{min} (Å)	r_{max} (Å)	r_{min} (Å)	r_{max} (Å)	r_{min} (Å)	r_{max} (Å)
15CuTe	1·55	2·35	1·55	2·40	2·30	3·20
20CuTe	1·60	2·30	1·55	2·35	2·30	3·25

3.2. Density

The densities of copper tellurite glasses containing 15 and 20 mol% of CuO were 5·61±0·05 and 5·66±0·05 g/cm^3, respectively, and the molar volume decreases from 26·31 to 25·37 cm^3/mol on increasing the CuO mol% due to the replacement of larger Te^{4+} (radius=0·66 Å) by smaller Cu^{2+} (radius=0·57 Å).[56] The addition of B_2O_3 (10 to 30 mol%) in copper tellurite

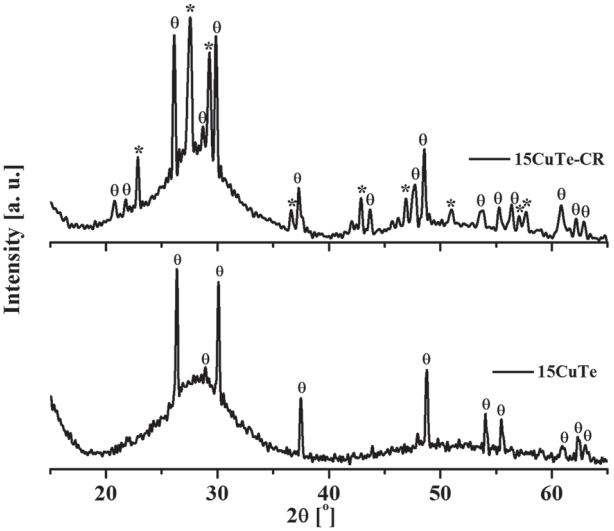

*Figure 1. XRD patterns of copper tellurite glass-ceramic sample before (15CuTe) and after annealing (15CuTe-CR). Peaks labeled as θ and * are due to tetragonal TeO_2 and monoclinic $CuTe_2O_5$ phases respectively*

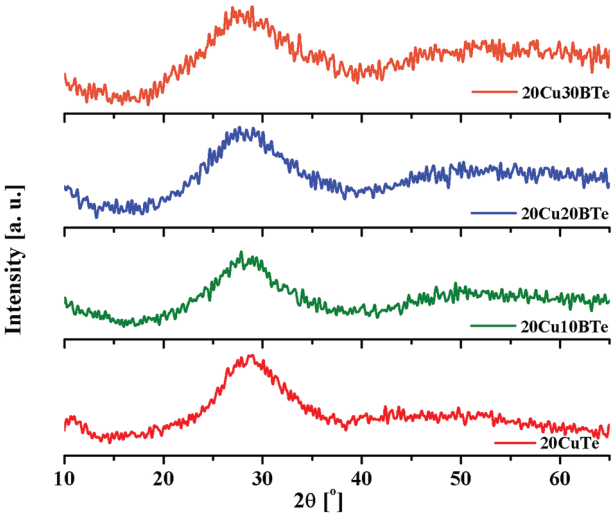

Figure 2. XRD patterns of copper tellurite and borotellurite glasses [Colour available online]

glasses further decreases the density from a value of 5·11±0·05 to 4·51±0·05 g/cm^3 and also decreases their molar volume. The decrease in density is due to the replacement of heavier TeO_2 (159·6 amu) by the lighter B_2O_3 (69·62 amu) (Table 1) while the molar volume decreases due to the replacement of larger Te^{4+} (0·66 Å) by the smaller B^{3+} (0·11 Å).[56] Both density and molar volume decrease with increase in B_2O_3 mol% in copper borotellurite glasses and similar effects are reported in other glass systems such as silver borotellurites and tungsten tellurites.[57,58]

3.3. Thermal properties

The DSC thermograms of copper tellurite and copper borotellurite glasses are shown in Figure 3. The glass transition temperature, T_g of copper tellurite glasses decreases from 306 to 301°C on increasing CuO concentration from 15 to 20 mol% due to lower bond enthalpy of Cu–O bonds (343 kJ/mol) as compared to that of Te–O bonds (391 kJ/mol).[59] The DSC scan of copper tellurite glass (20CuTe) shows single T_g and two crystallisation temperature peaks at 380°C (T_{c1}) and 457°C (T_{c2}) which can produce precipitates of $CuTe_2O_5$ and TeO_2 phases by the following thermal decomposition reaction:

$$20CuO{-}80TeO_2 \rightarrow 20CuTe_2O_5{+}40TeO_2 \quad (5)$$

The incorporation of B_2O_3 (10, 20 and 30 mol%) into copper tellurite glass (20CuTe) enhances the value of T_g from 325 to 366°C due to the formation of stronger B–O–Te linkages (B–O bond dissociation energy =807 kJ/mol) in place of the weaker Te–O–Te linkages (Te–O bond energy=391 kJ/mol).[59] The addition of B_2O_3 into 20CuTe glass sample suppresses the crystallisation tendency and the exothermic peaks at 464, 503 and 520°C are observed in glass samples: 20Cu10BTe, 20Cu20BTe and 20Cu30BTe, respectively. The thermal stability (resistance to crystallisation) of the copper borotellurite glasses enhances with increase in B_2O_3 concentration from 0 to 30 mol% (Table 2).

T_g shows a linear correlation with the average single bond energy (E_B) of glasses and the latter increases from a value of 381 to 506 kJ/mol (Figure 4 and Table 2) with increase in B_2O_3 from 0 to 30 mol%, E_B was calculated by the following formula:

$$E_B = \frac{20E_{Cu-O} + xE_{B-O} + (80 - x)E_{Te-O}}{100} \quad (6)$$

where, E_{Cu-O}, E_{B-O} and E_{Te-O} are the single bond dissociation energies of Cu–O (343 kJ/mol), B–O (807 kJ/mol) and Te–O (391 kJ/mol) bonds, respectively.[59] The important parameter that determines the value of glass transition temperature, is the average single bond dissociation energy, E_B, of the glass network.[60,61] DSC scans of copper tellurite and borotellurite glasses show a linear correlation between E_B and T_g as also found in other tellurite glass systems.[15,62,63] The

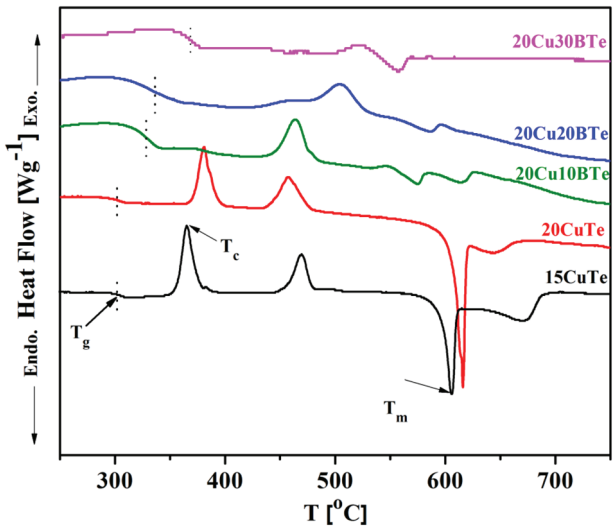

Figure 3. DSC scans of copper tellurite and borotellurite glasses [Colour available online]

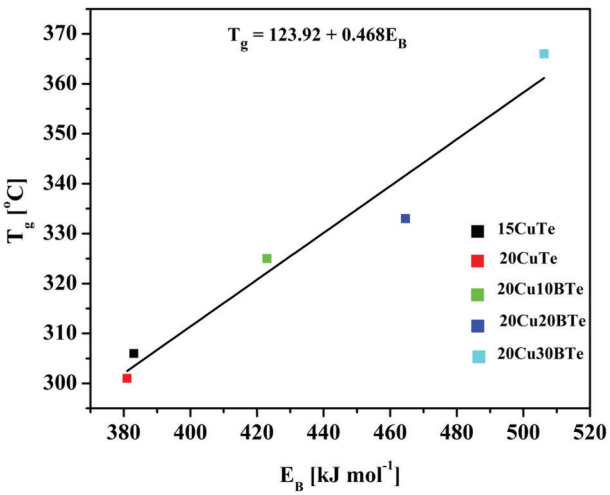

Figure 4. Variation of T_g with E_B in copper tellurite and copper borotellurite glasses [Colour available online]

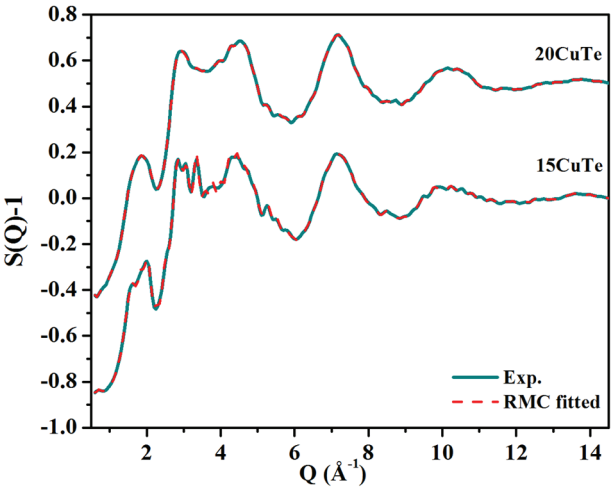

Figure 5. Experimental and RMC simulated (S(Q)-1) plots of copper tellurite glasses. The plot for sample 20CuTe is shifted by 0·5 units for clarity [Colour available online]

thermal stability, $\Delta T=(T_c-T_g)$ of the glasses increases from 80 to 154°C (Table 2) on adding 30 mol% B_2O_3 in the binary 20CuO–80TeO_2 glass. This confirms that the crystallisation tendency is suppressed by the addition of B_2O_3 due to increase in chemical disorder in the glass network.

3.4. Short range structure by neutron diffraction and RMC simulations

The (S(Q)−1) functions of the two copper tellurite glass samples calculated from RMC simulations matched well with the experimental ones and are shown in Figure 5. Although the copper tellurite sample with 15 mol% CuO has some crystalline precipitates of the tetragonal α-TeO_2 phase, it is predominantly amorphous and therefore the neutron diffraction studies provide reliable information about the structural transformations that occur with increase in CuO concentration from 15 to 20 mol% in the xCuO–(100−x)TeO_2 glass series.

The partial atomic pair correlation distributions $g_{Cu-O}(r)$, $g_{Te-O}(r)$ and $g_{O-O}(r)$ were obtained from the RMC modelling and these are displayed in Figure 6. The first peak is at 1·98±0·02 Å in both $g_{Cu-O}(r)$ and $g_{Te-O}(r)$ and the oxygen–oxygen pair correlation distribution, $g_{O-O}(r)$ shows maxima at 2·71±0·02 Å. It is known from neutron diffraction and molecular dynamics studies on amorphous TeO_2 that there are two types of Te–O linkages, the shorter ones at 1·880 Å are due to the Te–O linkages in the equatorial plane, while the longer ones at 2·121 Å are due to Te–O axial linkages and the average bond length is 2·000 Å.[9,14]

Neutron diffraction studies on the alkali and heavy metal oxide tellurite glasses found that the Te–O bond length distributions have a peak value at 1·95 Å,[43,64,65] which is in good agreement with the value of 1·96–1·98±0·02 Å for Te–O bond lengths found in the two copper tellurite glass samples. The average coordination number of Te with oxygen (N_{Te-O}) decreases from a value of 3·51±0·03 to 3·27±0·04 on increasing CuO concentration from 15 to 20 mol%. The Cu–O bond lengths are in the range: 1·96–1·98±0·02 Å (Table 5) and are in good agreement with the previous findings,[66] however, Cu^{2+} in tellurite glasses have tetra-

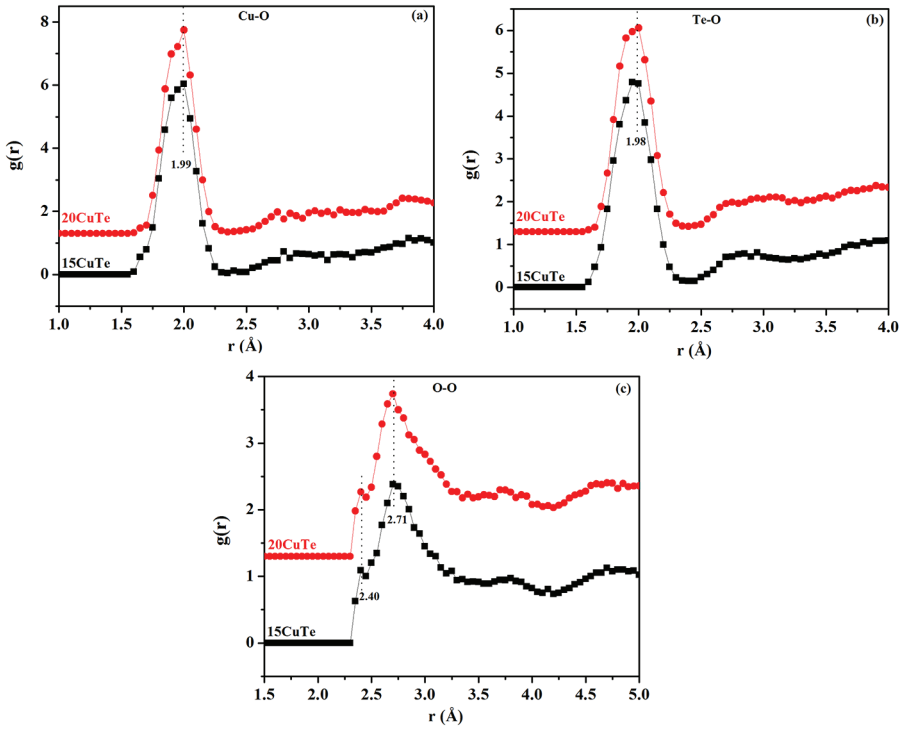

Figure 6. Pair distribution functions for (a) Cu–O, (b) Te–O and (c) O–O correlations in copper tellurite glasses. The plots for the sample 20CuTe are shifted by 1·3 units for clarity [Colour available online]

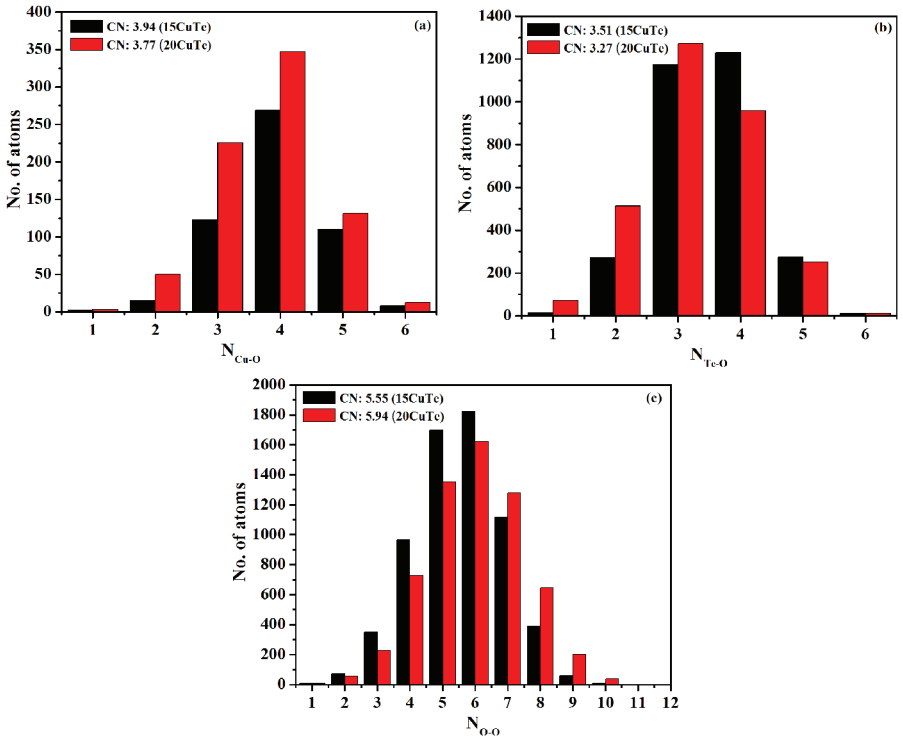

Figure 7. Distribution of (a) Cu–O, (b) Te–O and (c) O–O coordinations in copper tellurite glasses [Colour available online]

hedral coordination. Earlier it was found from the extended x-ray absorption fluorescence (EXAFS)[66] studies on goethite and humic acid containing Cu^{2+}, that the short equatorial nearest neighbouring distance for Cu–O bonds are in the range: 1·94–1·97 Å and that Cu^{2+} is in octahedral coordination. The average coordination of Cu^{2+} with oxygen (N_{Cu-O}) is 3·94±0·03 in the first sample (15CuTe) which confirms the existence of tetrahedral (CuO_4) units in copper tellurite glasses (Figure 7). N_{Cu-O} decreases to 3·77±0·02, similar to the decrease in N_{Te-O} with an increase in CuO content to 20 mol%. Hence nonbridging oxygens (NBO) are produced by the scissoring of both Cu–O and Te–O linkages. Raman results discussed below also indicate the transformation of TeO_4 into TeO_3 and TeO_{3+1} units containing NBOs.

Bhogi *et al*[20] and Rao *et al*[21] reported that Cu^{2+} ions in glasses can be in tetrahedral, octahedral and square planar coordination and that at high concentration of CuO (>0·6 mol%) mostly Cu^{+} ions exist. Duran *et al* reported that Cu^{2+} ions in oxide glasses produce green coloured samples.[67] In the present tellurite glass series, which contain a higher concentration of CuO (15 and 20 mol%) dark green coloured samples were formed, which indicates that Cu^{2+}, and not Cu^{+} exist in the glass network, although the exact determination of the oxidation state of copper will require an experimental measurement by XPS or EPR techniques.

Table 5. Structural properties of copper tellurite glasses from RMC simulations and Raman studies

		15CuTe	*20CuTe*
Nearest neighbour distance r_{ij} (Å)	Cu–O	1·96±0·02	1·99±0·01
	Te–O	1·98±0·03	1·96±0·02
	O–O	2·73±0·02	2·67±0·03
Bond angle θ_{ij} (°)	O–Cu–O	87·2±0·5	87·2±0·5
	O–Te–O	87·7±0·2	87·7±0·2
	O–O–O	58·0±1·2	58·0±1·2
Coordination number CN_{ij}	Cu–O	3·94±0·03	3·77±0·02
	O–O	5·55±0·28	5·94±0·38
	Te–O(neutron)	3·51±0·03	3·27±0·04
	Te–O(Raman)	3·49±0·01	3·44±0·01

The RMC studies on neutron data show that the Cu ions are mostly tetrahedrally coordinated with oxygen (N_{Cu-O}=3·94±0·03 in 15CuTe and 3·77±0·02 in 20CuTe). The Jahn–Teller distortion, therefore, modifies CuO_6 units into CuO_4 units, as found earlier by the EPR studies on phosphate glasses containing CuO.[32]

The bond angle distributions, θ_{O-Cu-O}, θ_{O-Te-O} and θ_{O-O-O} have maxima at 87·2±0·5°, 87·7±0·2° and 58·0±1·2°, respectively, and these curves are shown in Figure 8. It is known from the molecular dynamics simulations on the glassy-TeO_2, that the O–Te–O bond angle distributions have two peaks; the first weaker peak is in the range: 150–170° and is due to O_{ax}–Te–O_{ax} linkages while the second stronger peak in the range of 70–105° is due to O_{eq}–Te–O_{eq} and O_{eq}–Te–O_{ax} bonds.[16] The maxima at 87·7±0·2° in θ_{O-Te-O} distribution show that the majority of the linkages are O_{eq}–Te–O_{eq} and O_{eq}–Te–O_{ax} in TeO_3 units.[16] The second peak in the range: 150–160°, shows only a weak shoulder in both θ_{O-Cu-O} and θ_{O-Te-O}, therefore it is concluded that the concentration of O_{ax}–Te–O_{ax} and O_{ax}–Te–O_{ax} linkages is small in these glasses (Figure

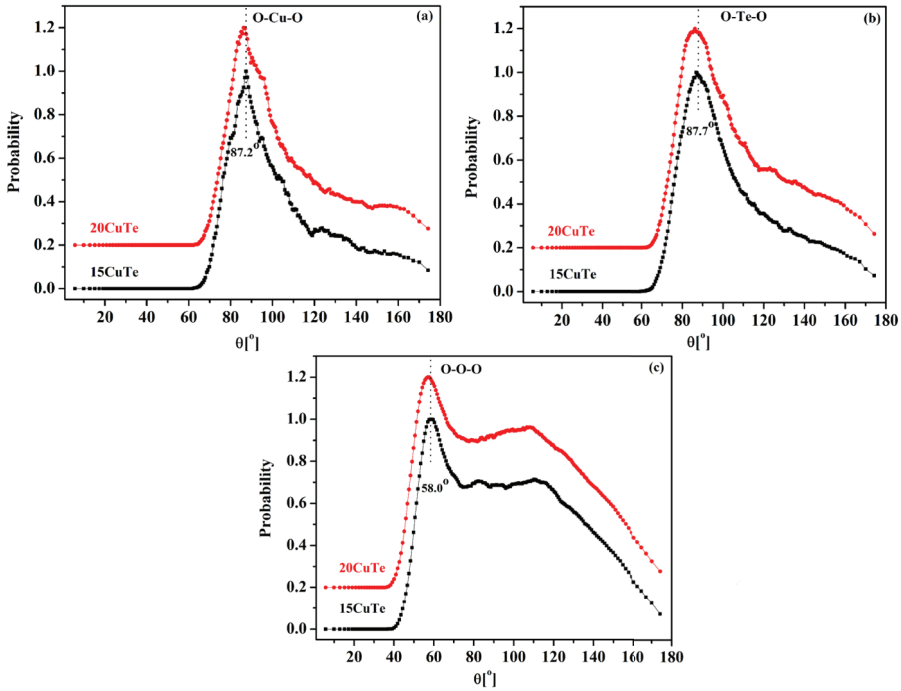

Figure 8. Bond angles distributions for (a) O–Cu–O, (b) O–Te–O and (c) O–O–O linkages in copper tellurite glasses. Plots for the sample 20CuTe are shifted by 0·2 units for clarity [Colour available online]

8). Similar bond lengths, coordination numbers, and bond angle distributions of Cu–O and Te–O linkages reveal that the two metal cations (Te^{4+} and Cu^{2+}) exist in the structural units of very similar geometry and size. The short range structural properties data of the tellurite samples are summarised in Table 5.

3.5. Te–O speciation by Raman spectroscopy

The Raman spectra of copper tellurite and copper borotellurite glasses are shown in Figure 9. These spectra show one strong peak at low phonon wavenumbers of ~55 cm^{-1}, a weak shoulder at 105 cm^{-1} and two distinctive Raman bands in the wavenumber ranges: 320–560 and 560–900 cm^{-1}. The Raman band: 590–900 cm^{-1} is due to asymmetric stretching vibrations of O–Te–O linkages in TeO_4 trigonal bipyramidal units (tbp) and TeO_3 trigonal pyramidal (tp) units. The band: 320 to 590 cm^{-1} is due to bending vibrations of Te–O–Te linkages.[16,58,68,69] The strong low frequency peak at 55 cm^{-1} is the boson peak which is the characteristic feature of glasses.[69–71] On increasing B_2O_3 concentration from 10 to 30 mol%, the peak at 663 cm^{-1} gets weaker and it reduces to a shoulder in glass with 30 mol% B_2O_3 concentration and the peak at 714 cm^{-1} shifts to higher frequencies i.e. 748 cm^{-1}. This confirms that the concentration of TeO_{3+1}, TeO_3 and TeO_3^{2-} (TeO_3 units containing two negatively charged NBOs) units increases with increase in B_2O_3 mol% due to the structural transformation: $TeO_4 \rightarrow TeO_3$. To compare the changes in Te–O speciation with the results from the neutron diffraction studies, Raman spectra were deconvoluted with Gaussian peaks centered at ~616, 659, 711 and 765 cm^{-1} (Figure 10) and the $N_{Te-O(Raman)}$ values were

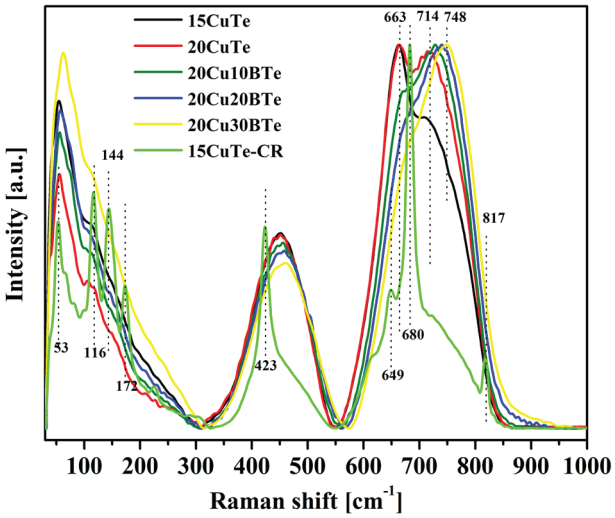

Figure 9. Raman spectra of copper tellurite and copper borotellurite glasses. Raman spectrum of the crystallised glass-ceramic sample (15CuTe-CR) is also displayed [Colour available online]

Table 6. Coordination of Te and B with O in xCuO–(100–x)TeO_2 and 20CuO–xB_2O_3–(80–x)TeO_2 glass series by Raman and ^{11}B MAS-NMR studies

Sample code	*$I_{(Raman)}$ Intensity ratio*	*$N_{Te-O(Raman)}$ (±0·03)*	*$N_{B-O(NMR)}$ (±0·01)*	*$N_{B-O(FTR)}$ (±0·03)*
15CuTe	0·49	3·49	-	-
20CuTe	0·44	3·44	-	-
20Cu10BTe	0·39	3·39	3·44	3·31
20Cu20BTe	0·36	3·36	3·41	3·22
20Cu30BTe	0·31	3·31	3·38	3·14

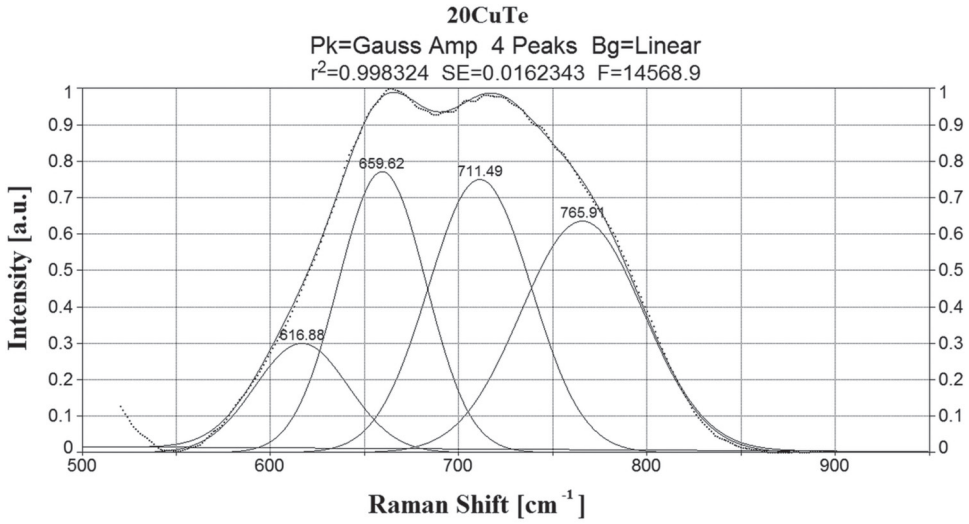

Figure 10. Deconvoluted Raman spectra of copper tellurite glass sample (20CuTe)

calculated by the following formula:[15,72]

$$N_{\text{Te–O(Raman)}} = 3 + \frac{I_4}{I_3 + I_4} \quad (7)$$

where I_4 is the sum of intensities of the peaks due to TeO_4 units (616 and 659 cm^{-1}), and I_3 is the sum of intensities of peaks due to TeO_3 and TeO_{3+1} units (711 and 765 cm^{-1}).

In case of xCuO–(100−x)TeO_2 samples, $N_{\text{Te–O(Raman)}}$ decreases from a value of 3·46±0·02 to 3·41±0·02 on increasing CuO concentration from 15 to 20 mol%. This result is consistent with RMC simulations of the neutron diffraction data, which showed that the Te–O coordination decreases from a value of 3·51±0·03 to 3·27±0·04.

In the case of copper borotellurite glasses, $N_{\text{Te-O(Raman)}}$ decreases from 3·39±0·01 to 3·31±0·01 on increasing the B_2O_3 concentration from 10 to 30 mol% (Table 6). This property of decrease in $N_{\text{Te–O}}$ with an increase in metal oxide concentration is a well known effect in tellurite glasses and it occurs with the addition of alkali, alkaline earth, rare earth and heavy metal oxides.[72–74]

The glass sample that was devitrified at 380°C for 4 h (15CuTe–CR), shows sharp Raman peaks at 53, 116 144, 172, 423, 649, 680, 817 cm^{-1} and a shoulder at 615 cm^{-1}. The peaks at 53, 116 144 and 172 cm^{-1} are due to the longitudinal optical vibrations of bridging oxygens of TeO_2[62,75] and peak at 423 cm^{-1} is due to the bending vibrations of Te–O–Te linkages. The shoulder at ~615 cm^{-1} shows the single degenerate symmetric vibrations of O–Cu–O linkages along with vibrations in TeO_4 units.[73,76] After the annealing treatment, the sharp peak at 683 cm^{-1} which corresponds to TeO_4 units becomes very prominent while the intensity of the band: 710–770 cm^{-1} (due to TeO_3 and TeO_{3+1} units) decreases significantly compared to its intensity in the parent glass sample (20CuTe). Therefore the devitrified sample (that contains a mixture of tetragonal TeO_2, monoclinic Cu_2TeO_5 and glassy phases) has a lower concentration of TeO_3 units and has higher average Te–O coordination compared to that in the parent glass sample.

3.6. B–O speciation by NMR

Figure 11 shows the ^{11}B MAS-NMR spectra of the three borotellurite glasses in the full chemical shift range of 150 to −150 ppm. The spectra show two central resonant peaks; the first peak at ~9 ppm and the second at ~0·5 ppm due to BO_3 and BO_4 structural units, respectively.[72,77,78] The two NMR peaks are broad and could not be resolved even at high magnetic field of 11·7 T due to the magnetic interactions of Cu^{2+} in the glasses.[21,22] These spectra also contain the two spinning side bands centred at approximately 95 ppm and −88 ppm. With the addition of B_2O_3 in copper tellurite glasses, the central resonance peak at 9 ppm becomes more intense, compared to the peak at ~0·5 ppm. This confirms the formation of more BO_3

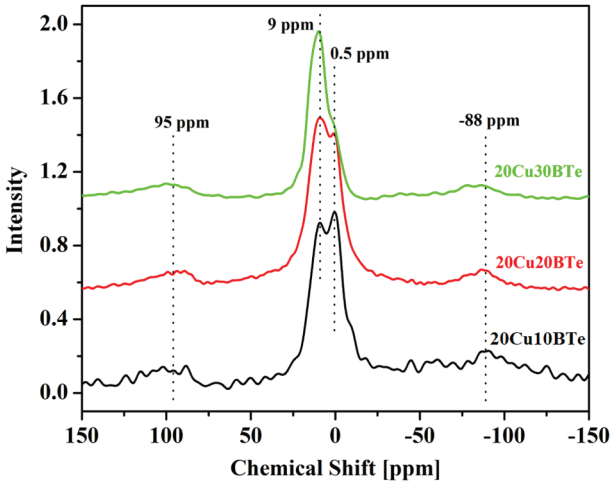

Figure 11. ^{11}B MAS-NMR spectra of copper borotellurite glasses [Colour available online]

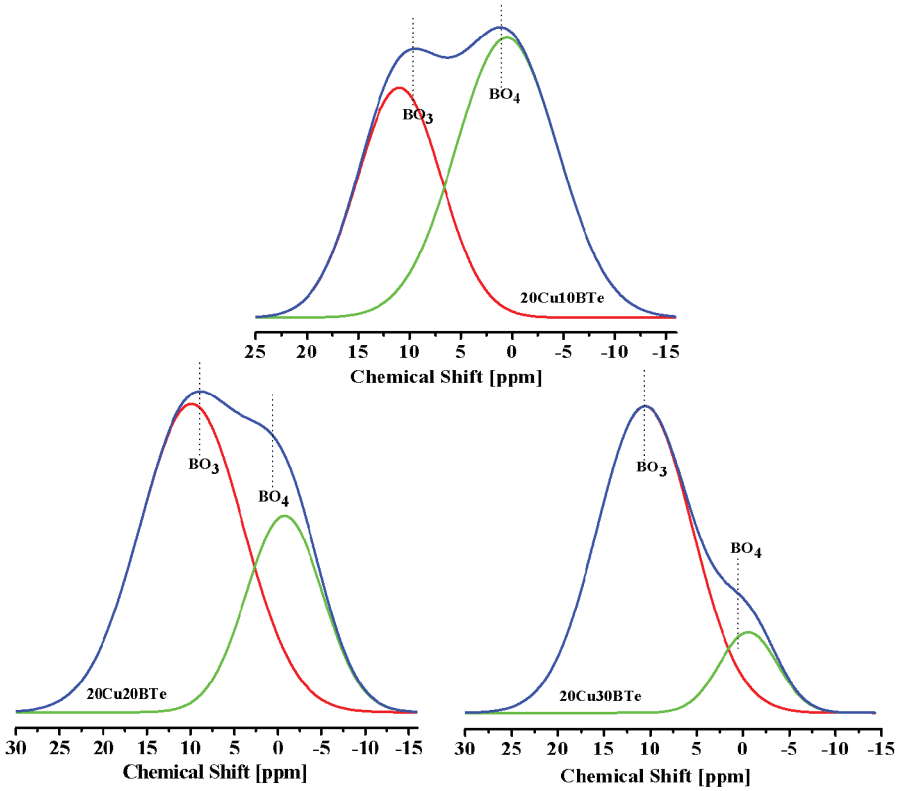

Figure 12. Deconvoluted ^{11}B MAS-NMR spectra of copper borotellurite glasses [Colour available online]

units with an increase in B_2O_3 concentration from 10 to 30 mol%. The MAS-NMR spectra were deconvoluted (Figure 12) and areas under the central and the two side-bands were used to determine the fraction of tetrahedral borons (N_4) in the borotellurite network, the coordination of boron with oxygen ($N_{B-O(NMR)}$) was calculated by following formula:[39]

$$N_4 = \frac{A_4}{A_3 + A_4} \quad (8)$$

$$N_{B-O(NMR)} = 3 + N_4 \quad (9)$$

A_3 and A_4 are the areas under the two resonant peaks of BO_3 and BO_4 units respectively in the central and the two sidebands. N_{B-O} decreases from 3·44 to 3·38 (Table 6) with an increase in B_2O_3 concentration from 10 to 30 mol%. The decrease in N_{B-O} is due to the structural transformation: $BO_4 \rightarrow BO_3$. The decrease in N_{B-O} is consistent with earlier studies on B–O speciation in borotellurite glasses.[39]

3.7. B–O speciation by FTIR

The FTIR absorption spectra of copper tellurite and copper borotellurite glasses are shown in Figure 13. Copper tellurite glasses show only one characteristic broad band from 520 to 900 cm^{-1} while the copper borotellurite glasses show two additional broad bands in the range: 1130–1550 cm^{-1} and 820–1130 cm^{-1} along with the band from 440–820 cm^{-1}. The broad band from 440–900 cm^{-1} is due to the stretching vibrations of Te–O–Te linkages in TeO_4 and TeO_3 and TeO_{3+1} units. The new band in the range: 820 to 1500 cm^{-1} arises on the incorporation of B_2O_3 in xCuO–(100–x)TeO_2 glasses is due to vibrations of B–O–B linkages in the borotellurite network. The band in the range: 820 to 1130 cm^{-1} is due to the B–O bond vibrations in BO_4 units while the band from 1130 to 1550 cm^{-1} is due to BO_3 structural units.[37] The addition of B_2O_3 up to 30 mol% in copper borotellurite glasses decreases the intensity of the absorption band in the range: 450 to 1130 cm^{-1} which confirms the decrease in the concentration of Te–O–Te linkages and BO_4 units. The concentration of tetrahedral borons in the glass

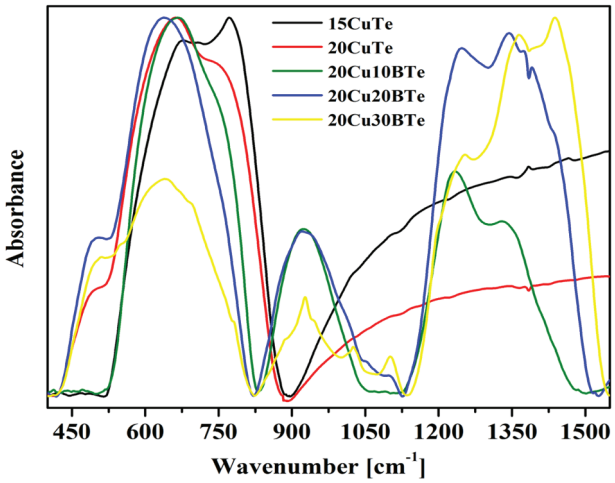

Figure 13. FTIR absorbance spectra of copper tellurite and borotellurite glasses [Colour available online]

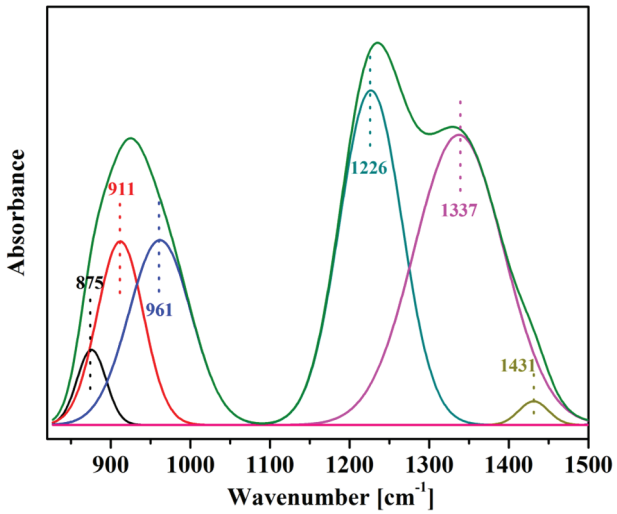

Figure 14. Deconvoluted FTIR spectra of copper borotellurite glass containing 10 mol% B_2O_3 [Colour available online]

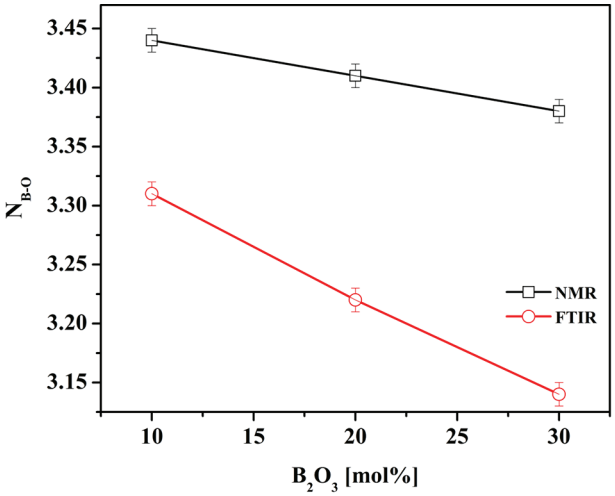

Figure 15. Variation of N_{B-O} with B_2O_3 mol% in copper borotellurite glass series [Colour available online]

network were also determined from FTIR studies, for this purpose the spectra in the wavenumber range: 820 to 1500 cm^{-1} was normalised, baseline corrected and fitted with Gaussian peaks centered at 875, 911, 961, 1226, 1337 and 1431 cm^{-1} (Figure 14). The areas under these peaks were used for the quantitative estimate of the fraction of tetrahedral borons, N_4 by the following formula:[39]

$$N_4 = \frac{A_4}{A_4 + A_3} \tag{10}$$

$$N_{B-O}=3+N_4 \tag{11}$$

where, A_4 and A_3 are the areas under the Gaussian peaks in the wavenumber range: 820 to 1130 cm^{-1} and from 1130 to 1550 cm^{-1}, respectively. The value of N_4 decreases from 0·31 to 0·14 on increasing B_2O_3 concentration from 10 to 30 mol%. This is due to the structural transformation: $BO_4 \rightarrow BO_3$ in xCuO–$y$$B_2O_3$–(100−$x$−$y$)$TeO_2$ glasses. The variation of N_{B-O} with B_2O_3 mol% in copper borotellurite glasses is shown in Figure 15.

4. Conclusions

The short range structure of copper tellurite and borotellurite glasses was studied by multiple techniques. Raman spectroscopy shows the structural transformation: $TeO_4 \rightarrow TeO_3$ on increasing CuO and B_2O_3 molar concentrations in the tellurite network. ^{11}B MAS-NMR and FTIR studies confirm that the fraction of tetrahedral borons in the borotellurite glass series decreases with an increase in B_2O_3 concentration. RMC simulations of the neutron diffraction data found that the nearest neighbor distances for Cu–O, Te–O and O–O bonds are 1·96–1·98±0·02 Å, 1·96–1·98±0·02 Å and 2·71±0·02 Å, respectively. Cu ions have tetrahedral coordination in the tellurite network due to Jahn–Teller effects, and the average Te and Cu coordination decreases with increase in CuO concentration from 15 to 20 mol%. CuO acts as network former in tellurite glasses and increase in its concentration enhances the thermal stability and the glass forming ability of the xCuO–(100−x)TeO_2 system. The average Te–O coordination is lower in the glassy phase as compared to that in the crystalline sample. A consistent picture of the short range structure of the tellurite and borotellurite network is found from the RMC simulations of the neutron diffraction data, Raman, ^{11}B MAS-NMR and FTIR studies.

Acknowledgments

Dr Margit Fábián, Centre for Energy Research, Hungarian Academy of Sciences, Budapest, Hungary is thanked for the providing training to the first two authors on the RMC technique at Guru Nanak Dev University under Indian National Science Academy and Hungarian Academy of Sciences mobility program in December 2015. The authors acknowledge UGC-DAE-Consortium for Scientific Research, Mumbai and Indore Centres, India for research grants that supported this work.

References

1. Manning, S. *A Study of Tellurite Glasses for Electro-optic Optical Fiber Devices*. School of Chemistry and Physics, PhD thesis, University of Adelaide, Adelaide, South Australia.
2. Yakhkind, A. K. Tellurite glasses. *J. Am. Ceram. Soc*., 1966, **49**, 670–5.
3. El-Mallawany, R. A. H. *Tellurite Glasses Handbook: Physical Properties and Data*. CRC Press, Boca Raton, 2002.
4. Jeansannetas, B., Blanchandin, S., Thomas, P., Marchet, P., Champarnaud-Mesjard, J. C., Merle-Méjean, T., Frit, B., Nazabal, V., Fargin, E., Le Flem, G., Martin, M. O., Bousquet, B., Canioni, L., Le Boiteux, S., Segonds, P. & Sarger, L. Glass structure and optical nonlinearities in thallium(I) tellurium(IV) oxide glasses. *J. Solid State Chem*., 1999, **146**, 329–35.
5. Kjeldsen, J., Yue, Y., Bragatto, C. B. & Rodrigues, A. C. Electronic conductivity of vanadium-tellurite glass-ceramics. *J. Non-Cryst. Solids*, 2013, **378**, 196–200.

6. Kjeldsen, J., Rodrigues, A. C., Mossin, S. & Yue, Y. Critical V_2O_5/TeO_2 ratio inducing abrupt property changes in vanadium tellurite glasses. *J. Phys. Chem. B*, 2014, **118**, 14942–8.
7. Zhang, Y., Wang, P., Zheng, T., Li, D., Li, G. & Yue, Y. Enhancing Li-ion battery anode performances via disorder/order engineering. *Nano Energ.*, 2018, **49**, 596–602.
8. Sekiya, T., Mochida, N. & Ogawa, S. Structural study of WO_3–TeO_2 glasses. *J. Non-Cryst. Solids*, 1994, **176**, 105–15.
9. Barney, E. R., Hannon, A. C., Holland, D., Umesaki, N., Tatsumisago, M., Orman, R. G. & Feller, S. Terminal oxygens in amorphous TeO_2. *J. Phys. Chem. Lett.*, 2013, **4**, 2312–16.
10. El-Mallawany, R. Structural interpretations on tellurite glasses. *Mater. Chem. Phys.*, 2000, **63**, 109–15.
11. Halimah, M. K., Daud, W. M., Sidek, H. A. A., Zaidan, A. W. & Zainal, A. S. Optical properties of ternary tellurite glasses. *Mater. Sci. Poland*, 2010, **28**, 173–80.
12. Yu, C., Yang, Z., Huang, A., Chai, Z., Qiu, J., Song, Z. & Zhou, D. Photoluminescence properties of tellurite glasses doped Dy^{3+} and Eu^{3+} for the ultraviolet and blue converted WLEDs. *J. Non-Cryst. Solids*, 2017, **457**, 1–8.
13. Santos, F. A., Figueiredo, M. S., Barbano, E. C., Misoguti, L., Lima, S. M., Andrade, L. H. C., Yukimitu, K. & Moraes, J. C. S. Influence of lattice modifier on the nonlinear refractive index of tellurite glass. *Ceram. Int.*, 2017, **43**, 15201–4.
14. Gulenko, A., Masson, O., Berghout, A., Hamani, D. & Thomas, P. Atomistic simulations of TeO_2-based glasses: interatomic potentials and molecular dynamics. *Phys. Chem. Chem. Phys.*, 2014, **16**, 14150–60.
15. Kaur, A., Khanna, A., González-Barriuso, M., González, F. & Chen, B. Short-range structure and thermal properties of aluminotellurite glasses, *J. Non-Cryst. Solids*, 2017, **470**, 14–18.
16. Gupta, N., Kaur, A., Khanna, A., Gonzàlez, F., Pesquera, C., Iordanova, R. & Chen, B. Structure-property correlations in TiO_2–Bi_2O_3–B_2O_3–TeO_2 glasses, *J. Non-Cryst. Solids*, 2017, **470**, 168–77.
17. Hoppe, U., Yousef, E., Rüssel, C., Neuefeind, J., Hannon, A. C. Structure of zinc and niobium tellurite glasses by neutron and x-ray diffraction. *J. Phys.: Condens. Matter*, 2004, **16**, 1645.
18. Salim, M. A., Khattak, G. D., Tabet, N. & Wenger, L. E. X-ray photoelectron spectroscopy (XPS) studies of copper–sodium tellurite glasses. *J. Electron Spectrosc.*, 2003, **128**, 75–83.
19. Pietrucci, F., Caravati, S. & Bernasconi, M. TeO_2 glass properties from first principles. *Phys. Rev. B*, 2008, **78**, 064203.
20. Bhogi, A., Vijaya Kumar, R. & Kistaiah, P. Effect of alkaline earths on spectroscopic and structural properties of Cu^{2+} ions-doped lithium borate glasses. *J. Non-Cryst. Solids*, 2015, **426**, 47–54.
21. Rao, L. S., Reddy, M. S., Rao, D. K. & Veeraiah, N. Influence of redox behavior of copper ions on dielectric and spectroscopic properties of Li_2O–MoO_3–B_2O_3: CuO glass system. *Solid State Sci.*, 2009, **11**, 578–87.
22. Upender, G., Prasad, M. & Mouli, V. C. Vibrational, EPR and optical spectroscopy of the Cu^{2+} doped glasses with $(90-x)TeO_2$–$10GeO_2$–xWO_3 ($7{\cdot}5 \leq x \leq 30$) composition. *J. Non-Cryst. Solids*, 2011, **357**, 903–9.
23. Kashif, I. & Ratep, A. Effect of copper oxide on structure and physical properties of lithium lead borate glasses. *Appl. Phys. A*, 2015, **120**, 1427–34.
24. Sandhya Rani, P. & Singh, R. Electrical and magnetic properties of copper tellurite glasses. *J. Mater. Sci.*, 2010, **45**, 2868–73.
25. Khattak, G. D., Mekki, A. & Wenger, L. E. Local structure and redox state of copper in tellurite glasses. *J. Non-Cryst. Solids*, 2004, **337**, 174–81.
26. Holloway, D. G. *Physical Properties of Glasses*. Wykeham Publications, London, 1973.
27. Yao, Z. Y., Möncke, D., Kamitsos, E. I., Houizot, P., Célarié, F., Rouxel, T. & Wondraczek, L. Structure and mechanical properties of copper–lead and copper–zinc borate glasses. *J. Non-Cryst. Solids*, 2016, **435**, 55–68.
28. Mouss, R. A., Krimi, S., Glorieux, B., Khattech, I., Couzi, M., Cardinal, T. & El Jazouli, A. Structural characterization and calorimetric dissolution behavior of Na_2O–CuO–P_2O_5 glasses. *J. Non-Cryst. Solids*, 2016, **452**, 144–52.
29. Falvello, L. R. Jahn–Teller effects in solid-state co-ordination chemistry. *J. Chem. Soc., Dalton Trans.*, 1997, 4463–76.
30. Wells, A. F. *Structural Inorganic Chemistry*, Fourth Edition, Clarendon Press, London, 1975.
31. Zachariasen, W. H. The atomic arrangement in glass. *J. Am. Chem. Soc.*, 1932, **54**, 3841–51.
32. Ravikumar, R. V. S. S. N., Rajagopal Reddy, V., Chandrasekhar, A. V., Reddy, B. J., Reddy, Y. P. & Rao, P. S.Tetragonal site of transition metal ions doped sodium phosphate glasses. *J. Alloys Compounds*, 2002, **337**, 272–6.
33. Tagiara, N. S., Palles, D., Simandiras, E. D., Psycharis, V., Kyritsis, A. & Kamitsos, E. I. Synthesis, thermal and structural properties of pure TeO_2 glass and zinc-tellurite glasses. *J. Non-Cryst. Solids*, 2017, **457**, 116–25.
34. Metwalli, E. Copper redox behavior, structure and properties of copper lead borate glasses. *J. Non-Cryst. Solids*, 2003, **317**, 221–30.
35. Khattak, G. D., Mekki, A. & Al-Shukri, A. X-ray Photoelectron spectroscopy study of copper tellurite glasses. *Phys. Scr.*, 2004, **70**, 187.
36. Ghosh, A. Electrical properties of semiconducting amorphous copper-tellurite glasses. *J. Phys.: Condens. Matter*, 1989, **1**, 7819.
37. Bürger, H., Vogel, W. & Kozhukharov, V. IR transmission and properties of glasses in the TeO_2–R_nO_m, R_nX_m, $R_n(SO_4)_m$, $R_n(PO_3)_m$ and B_2O_3 systems. *Infrared Phys.*, 1985, **25**, 395–409.
38. Ehrt, D. Structure, properties and applications of borate glasses. *Glass Technol.*, 2000, **41** (6), 182–5.
39. Kaur, N. & Khanna, A. Structural characterization of borotellurite and alumino-borotellurite glasses. *J. Non-Cryst. Solids*, 2014, **404**, 116–23.
40. Guillaume, E. & László, P. Reverse Monte Carlo modelling of the structure of disordered materials with RMC++ : a new implementation of the algorithm in C++. *J. Phys.: Condens. Matter*, 2005, **17**, S1.
41. McGreevy, R. L. & Pusztai, L. Reverse Monte Carlo simulation: a new technique for the determination of disordered structures. *Mol. Simul.*, 1988, **1**, 359–67.
42. Mellergard, A. & McGreevy, R. L. Reverse Monte Carlo modelling of neutron powder diffraction data, *Acta Crystallogr. A*, 1999, **55**, 783–9.
43. Neov, S., Gerasimova, I., Sidzhimov, B., Kozhukharov, V. & Mikula, P. Investigation of short-range atomic order in glasses from the MoO_3–TeO_2 system, *J. Mater. Sci.*, 1988, **23**, 347–52.
44. Ramesh Rao, N., Krishna, P. S. R., Basu, S., Dasannacharya, B. A., Sangunni, K. S. & Gopal, E. S. R. Structural correlations in Ge_xSe_{1-x} glasses – a neutron diffraction study. *J. Non-Cryst. Solids*, 1998, **240**, 221–31.
45. Salmon, P. S. & Zeidler, A. Networks under pressure: the development of in situ high-pressure neutron diffraction for glassy and liquid materials. *J. Phys.: Condens. Matter*, 2015, **27**, 133201.
46. Egami, T. & Billinge, S. J. L. *Underneath the Bragg Peaks: Structural Analysis of Complex Materials*. Elsevier, 2003.
47. Henry, E. F., Adrian, C. B. & Philip, S. S. Neutron and x-ray diffraction studies of liquids and glasses. *Rep. Prog. Phys.*, 2006, **69**, 233.
48. Fábián, M. & Cs, A. Basic network structure of SiO_2–B_2O_3–Na_2O glasses from diffraction and reverse Monte Carlo simulation. *Phys. Scr.*, 2016, **91**, 054004.
49. Fabian, M., Svab, E. & Krezhov, K. Network structure with mixed bond-angle linkages in MoO_3–ZnO–B_2O_3 glasses: neutron diffraction and reverse Monte Carlo modelling. *J. Non-Cryst. Solids*, 2016, **433**, 6–13.
50. Dawidowski, J., Granada, J. R., Santisteban, J. R., Cantargi, F. & Palomino, L. A. R. Appendix - neutron scattering lengths and cross sections. In: *Experimental Methods in the Physical Sciences*. Edited by F. Fernandez-Alonso & D. L. Price, Academic Press, 2013, pp. 471–528.
51. Fischer, H. E., Barnes, A. C. & Salmon, P. S. Neutron and x-ray diffraction studies of liquids and glasses. *Rep. Progr. Phys.*, 2005, **69,** 233.
52. Kaban, I., Jóvári, P., Hoyer, W. & Welter, E. Determination of partial pair distribution functions in amorphous $Ge_{15}Te_{85}$ by simultaneous RMC simulation of diffraction and EXAFS data, *J. Non-Cryst. Solids*, 2007, **353**, 2474–8.
53. Fábián, M., Sváb, E., Proffen, T. & Veress, E. Structure study of multi-component borosilicate glasses from high-Q neutron diffraction measurement and RMC modeling. *J. Non-Cryst. Solids*, 2008, **354**, 3299–307.
54. *Powder diffraction file*. 76-0679, ICDD, Newtown Square, PA, USA.
55. *Powder diffraction file*. 70-1312, ICDD, Newtown Square, PA, USA.
56. Dean, J. A. *Lange's Handbook of Chemistry*. McGraw-Hill, New York, 1999.
57. Kaur, A., Khanna, A., Gonzàlez, F. DSC and Raman studies of silver borotellurite glasses. *AIP Conf. Proc.*, 2016, **1731**, 070036.
58. Kaur, A., Khanna, A., Sathe, V., González, F., Ortiz, B. Optical, thermal, and structural properties of Nb_2O_5–TeO_2 and WO_3–TeO_2 glasses. *Phase Trans.*, 2013, **86,** 598–619.
59. Darwent, B. *National Standard Reference Data Series*, National Bureau of Standards, Washington, 1970, No. 31.
60. Tichý, L. & Ticha, H. Covalent bond approach to the glass-transition temperature of chalcogenide glasses. *J. Non-Cryst. Solids*, 1995, **189**, 141–6.
61. Dimitrov, V. & Komatsu, T. Polarizability, basicity and chemical bonding of single and multicomponent oxide glasses. *J. Chem. Technol.. Metall.*, 2015, **50**, 387–96.

62. Kaur, A., Khanna, A., González, F., Pesquera, C. & Chen, B. Structural, optical, dielectric and thermal properties of molybdenum tellurite and borotellurite glasses. *J. Non-Cryst. Solids*, 2016, **444**, 1–10.
63. Kumar, H. & Khanna, A. Structural, thermal and photoluminescent properties of Eu_2O_3–Li_2O–TeO_2 glasses. *J. Lumin*., 2018, **204**, 319–26.
64. Neov, S., Gerassimova, I., Krezhov, K., Sydzhimov, B. & Kozhukharov, V. Atomic arrangement in tellurite glasses studied by neutron diffraction, *Phys. Status Solidi A*, 1978, **47,** 743–50.
65. McLaughlin, J. C., Tagg, S. & Zwanziger, J. The structure of alkali tellurite glasses. *J. Phys. Chem. B*, 2001, **105,** 67–75.
66. Alcacio, T. E., Hesterberg, D., Chou, J. W., Martin, J. D., Beauchemin, S. & Sayers, D. E. Molecular scale characteristics of Cu(II) bonding in goethite–humate complexes. *Geochim. Cosmochim. Acta*, 2001, **65**, 1355–66.
67. Duran, A. & Fernandez Navarro, J. The colour of glass by Cu^{2+} ions. *Phys. Chem. Glasses*, 1985, **26** (4), 125–31.
68. Yadav, A. K. & Singh, P. A review of the structures of oxide glasses by Raman spectroscopy. *RSC Advances*, 2015, 5, 67583–609.
69. Kalampounias, A. G. Low-frequency Raman scattering in alkali tellurite glasses. *Bull. Mater. Sci*., 2008, **31**, 781–5.
70. Malinovsky, V. K. & Sokolov, A. P. The nature of boson peak in Raman scattering in glasses. *Solid State Commun*., 1986, **57**, 757–61.
71. Schroeder, J., Wu, W., Apkarian, J. L., Lee, M., Hwa, L.-G., Moynihan, C. T. Raman scattering and Boson peaks in glasses: temperature and pressure effects. *J. Non-Cryst. Solids*, 2004, **349**, 88–97.
72. Kaur, N., Khanna, A., Gónzález-Barriuso, M., González, F. & Chen, B. Effects of Al^{3+}, W^{6+}, Nb^{5+} and Pb^{2+} on the structure and properties of borotellurite glasses. *J. Non-Cryst. Solids*, 2015, **429**, 153–63.
73. Kaur, A., Khanna, A., Bhatt, H., Gónzález-Barriuso, M., González, F., Chen, B., Deo, M. N. B–O and Te–O speciation in bismuth tellurite and bismuth borotellurite glasses by FTIR, ^{11}B MAS-NMR and Raman spectroscopy. *J. Non-Cryst. Solids*, 2017, **470,** 19–26.
74. Kaur, A., Khanna, A. & Aleksandrov, L. I. Structural, thermal, optical and photo-luminescent properties of barium tellurite glasses doped with rare-earth ions. *J. Non-Cryst. Solids*, 2017, **476**, 67–74.
75. Ceriotti, M., Pietrucci, F. & Bernasconi, M. Ab initio study of the vibrational properties of crystalline α-TeO_2, β-TeO_2 and γ-TeO_2 phases. *Phys. Rev. B*, 2006, **73**, 104304.
76. Xu, J. F., Ji, W., Shen, Z. X., Tang, S. H., Ye, X. R., Jia, D. Z. & Xin, X. Q. Preparation and characterisation of CuO nanocrystals. *J. Solid State Chem*., 1999, **147**, 516–19.
77. Bajaj, A., Khanna, A., Chen, B., Longstaffe, J. G., Zwanziger, U. W., Zwanziger, J. W., Gómez, Y. & González, F. Structural investigation of bismuth borate glasses and crystalline phases. *J. Non-Cryst. Solids*, 2009, **355**, 45–53.
78. Zhong, J. & Bray, P. J. Change in boron coordination in alkali borate glasses, and mixed alkali effects, as elucidated by NMR. *J. Non-Cryst. Solids*, 1989, **111**, 67–76.